# Modeling the Mass Transfers During the Elaboration of Chitosan-Activated Carbon Composites for Medical Applications

**A. Venault, D. Bouyer, C. Pochat-Bohatier, and C. Faur**
UMR Cirad 016-Génie des Procédés - Eau - Bioproduits, Université de Montpellier 2, place Eugène Bataillon, 34095 Montpellier Cedex 5, France

**L. Vachoud**
UMR Cirad 016-Génie des Procédés - Eau - Bioproduits, UFR Sciences Pharmaceutiques et Biologiques, 15 avenue Charles Flahault, BP 14491, 34093 Montpellier Cedex 5, France

*DOI 10.1002/aic.12078*
*Published online October 23, 2009 in Wiley InterScience (www.interscience.wiley.com).*

*Hydrogels composites composed of chitosan and activated carbon were prepared for medical applications using the vapor-induced phase separation process. Since the gelation process involves mass exchanges between the polymer solution and the air, the kinetics of mass transfer were investigated through experimental and modeling approaches. Among the formulation and process parameters, gravimetric measurements exhibited that mass transfers were mostly controlled by the initial ammonia partial pressure. A nonisotherm mass-transfer model was developed to predict the nonsolvent and solvent exchange rates, therefore, the water and ammonia concentration profiles within the sample during the process. The numerical results were successively validated with gravimetrical kinetic curves obtained in a chamber where the process parameters were controlled. The model aimed also at predicting the pH moving front along the film thickness. The gelation time could also be predicted for different operating conditions (formulation and process parameters).* © 2009 American Institute of Chemical Engineers *AIChE J,* 56: 1593–1609, 2010
*Keywords: composite hydrogels, VIPS process, mass transfers, mathematical modeling*

## Introduction

Chitosan is the deacetylated form of chitin, a natural biopolymer mostly extracted from the shells of crustaceans. After a treatment with concentrated sodium hydroxide or potassium hydroxide, amino groups are produced along the initial chitin chain structure leading to chitosan. Thus, the main difference between chitin and chitosan comes from the degree of acetylation (DA). Below 60%, the polymer is called chitosan, whereas it is termed chitin for DA over 60%.[1,2] Due to its numerous biological properties, this polymer is widely studied in the field of wound healing dressings.[3–6] Thus, it has been proven that chitosan under the hydrogel form could be efficient to cure burns, and that this material was well tolerated and promoted a good tissue regeneration.[7]

Activated carbon (AC) is obtained by heat treatment of various natural precursors (coal, peat, coconut and wood). A physical thermal oxidation (pyrolysis followed by an oxidation by steam), or a chemical one (impregnation by a mineral agent followed by a pyrolysis), enables to develop a high-specific surface, going from 500 to 2,000 $m^2/g$.[8] The internal structure of AC is constituted by micropores (diameter of pores lower than 2 nm) and mesopores (between 2 and

Correspondence concerning this article should be addressed to A. Venault at avenault@univ-montp2.fr.

50 nm). In addition to this porous structure, activated carbon presents oxygen functional groups at the periphery of carbon layers, which may be involved in adsorption mechanisms.[9,10]

Composite hydrogels made of both chitosan and AC have not been studied yet in the medical field. However, a few works mention the use of this composite for water treatment applications. Thus, chitosan-encapsulated AC beads were prepared to adsorb dyes and humic acid from aqueous solutions.[11] The Cr (VI) removal from synthetic wastewater using activated carbon modified with chitosan was also studied.[12] Besides, the same kind of adsorbent was used to remove heavy metals from industrial wastewater.[13] As the feasibility of chitosan-AC composites has been successfully investigated in water treatment applications, it is believed that it would also be of great interest to use these composites for another application related to the medical field: the wound dressings. Depending on their structure and composition, some dressings may simply absorb exudates, while others may inhibit the colonization of microorganisms, but the search for a material that eliminates both odor and exudates still continues. Actually, chitosan would be used for its numerous biological properties among which its bioactivity, its bioresorbability and its biocompatibility. The application of chitosan hydrogel would interact with and protect the wound ensuring a good, moist healing environment.[14–19] AC, an efficient adsorbent, would permit to adsorb organic molecules responsible for unsuitable odors. These are the different small molecules such as short chain organic acids or amines like cadaverine or putrescine representing a major problem for patient.[20,21] Its role would be to ensure an effective odor control. Finally, chitosan-AC hydrogels would permit to eliminate both exudates and odors. Over the past 30 years, different odor controlling dressings have been produced. A comparative study of adsorption performances was even carried out by Thomas et al.[20] However, at present, there is no product which associates in the same dressing biological properties and adsorption properties of odors. Nevertheless, recent studies interested in chitosan-carbon nanotubes hybrid materials for future biomedical applications.[22,23] According to these studies, the goal would be to combine the properties of the materials. However, both AC and carbon nanotubes are very different adsorbents leading to different types of composites with chitosan.

To prepare chitosan hydrogels, the most commonly used process is the wet process also called the immersion/precipitation process.[24–28] It consists in solubilizing the polymer in an acidic aqueous solution, the acetic acid, most of the time.[29] In a second step, the polymeric solution has to be submitted to a basic media (sodium hydroxide) to induce the gelation. The use of an enzymatic process is also mentioned in literature, but it is not as widespread as the previous one for chitosan gelation.[30] In this case, the basic media permitting the gelation to occur is produced *in situ*. Some rare works also mention the chitosan gelation from gaseous ammonia.[7,31] This process is the so-called vapor-induced phase separation (VIPS) process, mainly used to prepare organic membranes and films from synthetic polymer.[32–35] In this process, nonsolvent vapors penetrate the polymeric solution and induce the phase separation. It leads to the film formation with specific pore characteristics depending on several parameters among which the polymer concentration,[34] the nonsolvent partial pressure in the nonsolvent atmosphere,[33,35] and the exposure time to the nonsolvent vapors.[31,35]

The main advantage of the VIPS process is to slow down the mass transfers involved in the film formation, compared to more classical elaboration processes such as the wet process for which the liquid/liquid transfers involve fast solvent-nonsolvent exchanges. Furthermore, using the VIPS process induces lower solvent extraction rate from the polymeric system, and is responsible for slower gel formation; indeed, the polymer chains stay into contact with a good solvent during a longer time than for the wet process. In addition, the VIPS process allows a better control of the mass-transfers mechanisms, and, therefore, of the gel structuring, which is crucial considering the targeted application: the wound dressings. With regards to this application, such hydrogels should be composed of several layers.[3] A porous layer, in contact with the wound, allows maintaining a perfect humidity above it and an efficient drainage of the exudates. A dense layer, in contact with the atmosphere, prevents a hypothetic bacterial infection to occur. Nevertheless, it still permits the gas transfers and more specifically the oxygen transfer, which is necessary to healing. Using the VIPS process makes possible to prepare at least the homogeneous cellular porous layer which will permit water and exudates exchanges since this kind of structure has already been observed for synthetic polymers.[33,37,38]

Although there is no study reported in the literature concerning the modeling of a natural polymer gelation using nonsolvent vapors, several works focussed on the modeling of the vapor induced phase separation for thin films fabrication. Such modeling studies used the Flory-Huggins theory to describe thermodynamics and multi-component diffusivities, in order to simulate the mass transfers within the film. A first isotherm mass transfer model was developed for the ternary poly(vinylidene fluoride)/dimethyl formamide/water system which aimed at predicting the evolution of the concentration profile during the film formation.[39] Then, another isotherm model was developed for the quaternary water/N-methylpyrrolidone (NMP)/poly(ether sulfone) (PES)/polyvinyl pyrrolidone (PVP) system.[40] This model helped to better understand the classical asymmetric structures observed in the membranes. Later, a nonisotherm model was developed to integrate the coupling between mass and heat transfers. It was applied for four different systems: cellulose acetate/acetone/water, (vinylidene fluoride)/dimethyl formamide/water, polysulfone/*N*-methyl-2-pyrolidone/water and poly (ether imide)/*N*-methyl-2-pyrolidone/water.[41] The effect of the process parameters (relative humidity, air flow rate, temperature) was investigated. Nevertheless, these works involved only water as the nonsolvent, because all polymers were highly soluble in an organic media and so, very hydrophobic. Moreover, the membrane formation did not involve a chemical reaction.

To the best of our knowledge, the preparation of hydrogels from natural polymer with a control of the process parameters (temperature, nonsolvent partial pressure) meaning a control of the final structure in terms of porosity was never carried out. Moreover, the modeling approach was never applied to the gelation process induced by nonsolvent vapors. The scope of this work is also to better quantify the mass-transfer rates during the gelation process by comparing

**Table 1. Physicochemical Properties of Chitosan**

| Producer | Batch Number | DA (%) | Viscosity (*) at 298 K (Pa·s) | $M_w$ (g/mol) |
|---|---|---|---|---|
| France Chitine | 342 | 20 | 0.1 | 180,000 |

DA: acetylation degree; $M_w$: molecular weight in weight; (*) given by the producer.

numerical and experimental data. The first part of this article presents the model which includes a coupling between mass and heat transfers. The numerical results are then validated using gravimetric data performed inline during the process. Last, the model is used to (1) predict the concentration profiles within the polymer solution during the gelation, (2) to follow the pH moving front along the film thickness, and (3) to quantify the gelation time that depends on the process parameters.

## Methodology

### *Materials*

*Chitosan and Active Carbon.* Chitosan produced from shrimp shell wastes (batch N° 342) was supplied by France Chitine Co. (France). It has a 20% degree of acetylation (producer data and proton magnetic nuclear resonance measurement). Molecular weights were assessed by size exclusion chromatography and multiangle laser light scattering (MALLS) using TSK-gel G-4000 PWXL and G-6000 PWXL columns and an IsoChrom LC pump (Spectra Physics). The columns are connected to a Waters 410 (Waters-Millipore) differential refractometer. $CH_3COOH$-ammonium acetate buffer at pH 4.3 is used as eluent. The MALLS detection was obtained by means of a Wyatt Dawn F detector on line, operating at 632.8 nm. The polymer solutions (0.1% w:v) were filtered on a 0.22 $\mu$m pore-size cellulose acetate membrane (Millipore) before injection by means of an injection loop (50 $\mu$m). Properties of chitosan are given in Table 1.

Powdered active carbon used in this study is a commercial product from the Pica Co. (St Maurice, France). Its pore characteristics were determined from $N_2$ adsorption isotherms at 77 K performed with a Micromeritics 2010 analyzer after degas for 48 h at 573 K. The theories of Brunauer et al., Horvath and Kawazoe, and Barrett et al. were used to calculate specific surface area, micropore volume and mesopore-size distribution, respectively.[42–44] The pH at which the activated carbon surface has no charge (pH at the point of zero charge or $pH_{PZC}$) is another important feature. Its determination was carried out according to the so-called pH drift method: 100 $cm^3$ of distilled water solution was placed in erlenmeyer flasks, and the pH was adjusted to a value between 1 and 13 by adding HCl or NaOH 0.1 mol/L. Then a weight of 0.1 g of active carbon was added, and the final pH was measured after stirring during 24 h at 293 $\pm$ 2 K. The $pH_{PZC}$ is the point where the curve $pH_{final}$ vs. $pH_{initial}$ crosses the line $pH_{final} = pH_{initial}$.[45] Finally, the surface acidity and basicity of AC particles were quantified using the Boehm methodology. These parameters were determined for two main reasons. First, acetic acid has to be used to solubilize chitosan. The acetic acid amount must be as close as possible as the stoechiometric one, to avoid the polymer hydrolysis that might occur when the acid is used in large excess.[29,46] Thus, the required amount of acid had to be calculated considering both the amino-groups on the chitosan and the basic groups on AC particles surface. Second, acid functions might influence the concentration gradient of the basic media used to induce the polymer gelation. Characteristics of the AC used are given in Table 2.

## Methods

### *Preparation of solutions*

The methodology used to prepare the composite solutions was described in detail in previous work.[28] Briefly, chitosan solutions were obtained by dissolving chitosan powder, mixed with AC powder, in an acetic acid solution (Laurylab) to achieve protonation of the polymer. The final chitosan concentration ranged from 3 to 4% (w:v), whereas the AC concentration was lower, between 0 and 1.3% (w:v). The mixture was then stirred for 24 h and stored at 4°C.

During this step, the chemical reaction involved is as follows

$$Chit\text{-}NH_2 + AcOH \Leftrightarrow Chit\text{-}NH_3^+ + AcO^- \quad (1)$$

where $Chit\text{-}NH_2$ is the chitosan under insoluble form. It reacts with acetic acid ($AcOH$) to produce $Chit\text{-}NH_3^+$, the quaternium chitosan soluble in water and the acetate ion ($AcO^-$).

### *Preparation of hydrogels using the VIPS gelation process*

The process is composed of four main elements (Figure 1). A double walled chamber (Legallais, France) was specially designed for this application. An external heater, made of a water bath, permits to set and keep constant the temperature inside the chamber containing the diluted ammonia solution. The ammonia vapors will induce the gelation of the chitosan solution by successive absorption-diffusion mechanisms. The composition of the gaseous phase above the gel remains the same because the temperature is well controlled and the chamber is closed. Initial relative humidity was also measured for each experiment and ranged between 96 and 98% $\pm$ 1%. A balance (Precisa XB 320 M, Balco) is placed below the chamber and allows following inline the sample weight during the process. Finally, a data acquisition system

**Table 2. Physicochemical Properties of Active Carbon**

| Producer | Diameter ($\mu$m) | $S_{BET}$ ($m^2$/g) | $V_p$ ($cm^3$/g) | % micropore volume | $pH_{PZC}$ | Basic Functions (mol/g) | Acid Functions (mol/g) |
|---|---|---|---|---|---|---|---|
| Pica | 5–60 | 1,744 | 1.13 | 25 | 9.8 | $8.9\ 10^{-4}$ | $2.9\ 10^{-3}$ |

$S_{BET}$: specific surface area; $V_p$: pore volume; $pH_{PZC}$: pH at the point of zero charge.

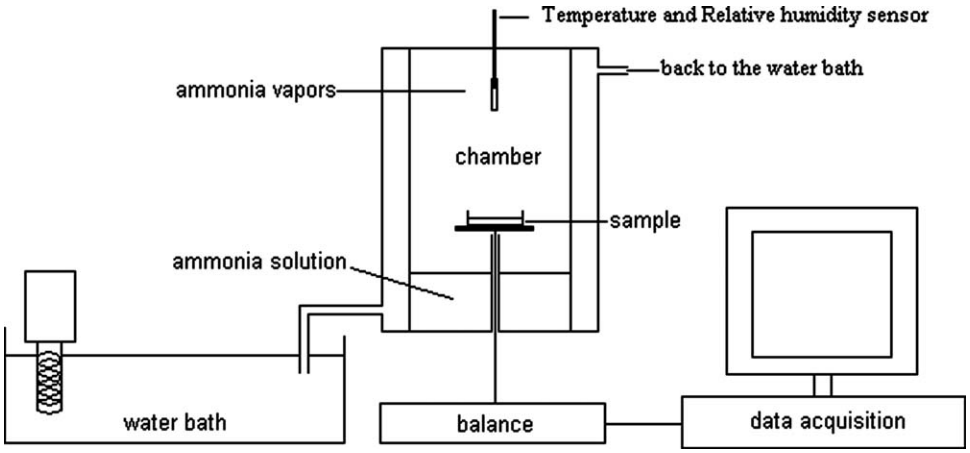


**Figure 1. Schematic of the VIPS reactor used in this work.**

(Balint) records the mass variations at predefined time steps. These mass variations should be mainly due to the solvent (water) and nonsolvent (ammonia) exchanges. Ammonia is the gelation agent and is first absorbed at the air-solution interface before transferring by diffusion toward the bottom of the sample.[31] Consequently, a global mass intake is expected to occur, as it has been previously reported in the case of membranes formation by the VIPS process.[33,35] Water transfer could also be involved in the global mass variation, since it could evaporate depending on the ratio between the water chemical potential in the solution and in the gas phase (directly linked to the relative humidity). Nevertheless, the driving force to this transfer by evaporation should be quite weak in this work because of both the high-water content in hydrogels, and high-relative humidity in the gas phase. Finally, a syneresis phenomenon, linked to the water transfer, and, thus, to a mass variation, might be expected.[47]

To prepare the hydrogels, 5 ($\pm$0.1) g of the polymeric solution were poured into a 5 cm inner dia. Petri dish, and then exposed to ammonia vapors in the closed chamber. The inner atmosphere of the chamber was presaturated with ammonia vapors for 1 h before starting the gelation process. The exposure time to vapors ranged from 4 to 24 h depending on the experiment. Final thickness was about 2.5 mm. Then, the samples were rinsed with deionized water and stored in deionized water at 277 K until use.

The different operating conditions used to prepare the gels are gathered in Table 3.

### *Environmental scanning electron microscopy observations*

The produced gels were observed by a Phillips XL 30 environmental scanning electronic microscope (Figure 2). Whatever the formulation, the polymeric matrix is composed of symmetric cellular pores (diameter $<$20 $\mu$m). These pores should allow a control of the relative humidity above the skin, which is required for an efficient healing. In addition, activated carbon seems to be homogeneously distributed within the composite, permitting to avoid breaking points that might be responsible for a low-mechanical strength of the composites.

## Theory

### *Geometry and assumptions of the model*

The geometry considered for the model is illustrated in Figure 3. The initial liquid system consists of chitosan and AC in an acetic acid solution. This liquid system is cast onto a glass Petri dish placed on the stainless steel plate of the balance. Gelation from ammonia vapors is governed by a perpendicular flux. The solvent (water) may simultaneously evaporate from the system in a perpendicular direction. The gas phase over the system is characterized by the bulk temperature $T_b$ (K), the relative humidity, $RH$ (%), the vapor pressure of each volatile compound $P_{vi}$ (Pa), and the heat-transfer coefficient $h_b^{up}$ (W/m$^2$·K). Concerning the gas phase next to the bottom of the Petri dish, it is characterized by $T_b$, $RH$ and $h_b^{down}$.

The basic assumptions of the model are (1) one-dimensional (1-D) diffusion; (2) no chitosan nor AC transfer to the air side; (3) uniform temperature throughout the system; (4) ideal gas behavior at the air side; (5) gas-liquid equilibrium at the air-film interface; (6) no chitosan nor AC interactions on the activity of the other species; and (7) no chitosan nor AC interactions on the transport mechanisms.

### *Thermodynamic model*

The thermodynamic model used in literature for ternary component system is based on the Gibbs free energy of mixing, expressed according to the Flory-Huggins theory.[40,41] In these works, the classical polymer concentration used for preparing porous or dense membrane ranged from 10 to 30%

**Table 3. Process Parameters**

| Gel | Ammonia Concentration in the Liquid Phase (% p:p) | Temperature of the Bulk (K) | Relative Humidity (%) | Exposure Time to Vapors (h) |
|---|---|---|---|---|
| A | 1.625 $\pm$ 0.001 | 303.15 $\pm$ 0.5 | 98 $\pm$ 1 | 24 |
| B | 1.625 $\pm$ 0.001 | 303.15 $\pm$ 0.5 | 97 $\pm$ 1 | 24 |
| C | 0.875 $\pm$ 0.001 | 293.15 $\pm$ 0.5 | 96 $\pm$ 1 | 4 |
| D | 1.625 $\pm$ 0.001 | 293.15 $\pm$ 0.5 | 98 $\pm$ 1 | 6.5 |
| E | 1.625 $\pm$ 0.001 | 313.15 $\pm$ 0.5 | 98 $\pm$ 1 | 4 |
| F | 1.625 $\pm$ 0.001 | 293.15 $\pm$ 0.5 | 97 $\pm$ 1 | 6.5 |

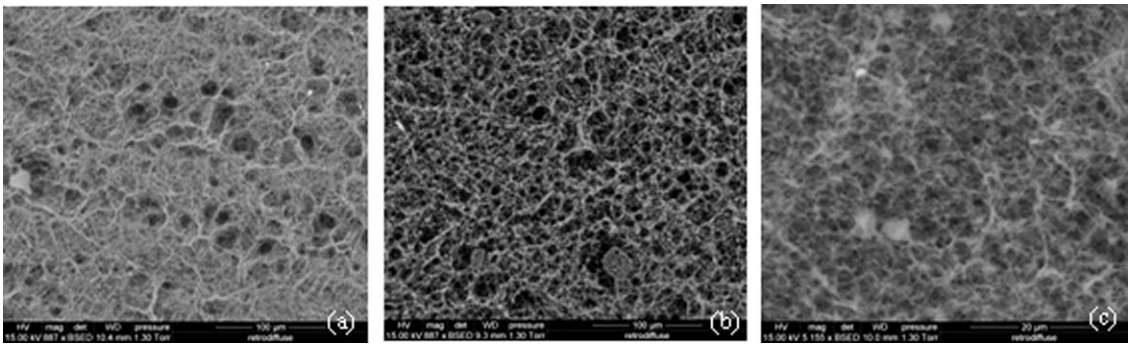

**Figure 2. ESEM observations of the composite hydrogels.**

(a) Surface observation, [chitosan] = 4% (w:v), [AC] = 0% (w/v), (b) surface observation, [chitosan] = 4% (w:v), [AC] = 1.3% (w/v), and (c) cross section observation, [chitosan] = 4% (w:v), [AC] = 1.3% (w/v).

in weight. In this case, the polymer concentration is dramatically lower, since it ranges from 3 to 4% w:v. Consequently, it is relevant to expect that the polymer does not strongly affect the water chemical potential in the solution. In addition, as far as we know, data such as the interaction parameters between chitosan and water and between chitosan and ammonia have not been reported. Hence, another thermodynamic model was adopted to describe the gas/polymeric system interface equilibrium: the ammonia ($NH_3$) vapor-liquid equilibrium. The numerical data related to the partial pressure of $NH_3$ over aqueous solutions of $NH_3$, depending on the mass fraction of ammonia and the temperature, were found in literature.[48]

### *Mass-transfer model coupled to chemical reactions*

When ammonia vapors penetrate into the polymer solution, ammonia first reacts with acetic acid that was initially mixed with chitosan with a slight excess to perfectly solubilize the polymer. Then, ammonia reacts with chitosan. This reaction involves a proton transfer from the quaternium chitosan ($Chit\text{-}NH_3^+$), formed during previous solubilization of chitosan in acidic media, to the base ($NH_3$) leading to the gel matrix formation ($Chit\text{-}NH_2$), and to the ammonium ion ($NH_4^+$). Reaction 2 (Eq. 2) occurs before reaction 3 (Eq. 3) because $AcOH$ is a stronger acid than $Chit\text{-}NH_3^+$ ($K_{a,(AcOH/AcO-)} = 10^{-4.75}$ vs. $K_{a,(Chit\text{-}NH3\ +/Chit\text{-}NH2)} = 10^{-6.5}$)

$$AcOH + NH_3 \Leftrightarrow AcO^- + NH_4^+ \tag{2}$$

$$Chit\text{-}NH_3^+ + NH_3 \Leftrightarrow Chit\text{-}NH_2 + NH_4^+ \tag{3}$$

Seven species are, thus, involved in mass-transfer model, coupled to chemical reactions, considering Eqs. 2 and 3, and water, the main component of the hydrogels.

Although the acid/base reactions should not represent the limiting step of the whole process, they were taken into account to ensure a better modeling of the mass-transfer mechanisms.[49]

The local continuity equation for each component can be written as follows, if assuming binary Fickian diffusion within the matrix

$$\frac{\partial \rho_i}{\partial t} + \nabla(-D_{i/m}\nabla\rho_i) = R_i \quad \text{i} = 1 \text{ to } 7 \tag{4}$$

where $\rho_i$ (kg/m$^3$) is the local concentration of component $i$, and $D_{i/m}$ (m$^2$/s) is its mutual diffusion coefficient within the matrix. $R_i$ is a reaction term. Subscripts ($i$) refer to (1) $NH_3$, (2) $H_2O$, (3) $Chit\text{-}NH_3^+$, (4) $Chit\text{-}NH_2$, (5) $AcOH$, (6) $AcO^-$, and (7) $NH_4^+$. The assumption of binary Fickian diffusion was consistent since the polymer and the AC concentrations are very low ($\leq$4% w:v and $\leq$1.3% w:v, respectively), therefore, they were assumed not to influence the water and ammonia transport phenomena.[50]

However, in this work, $Chit\text{-}NH_3^+$ and $Chit\text{-}NH_2$ were supposed not to take part in diffusion phenomena since the diffusion of the polymer chains was assumed to be negligible. For both species, Eq. 4 can be simplified as follows

$$\frac{\partial \rho_i}{\partial t} = R_i \tag{5}$$

As water is not involved in the chemical reactions, its specific continuity equation can be simplified

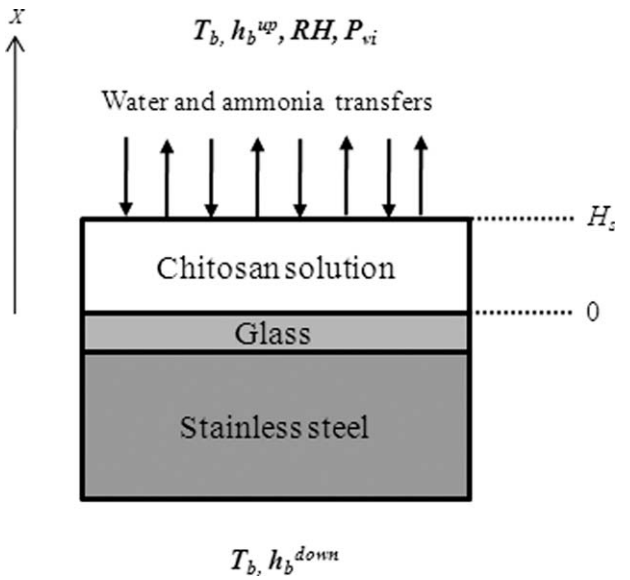


**Figure 3. Schematic of the model.**

$$\frac{\partial \rho_2}{\partial t} + \nabla(-D_{2/m}\nabla\rho_2) = 0 \quad (6)$$

Considering a general reversible system involving $j$ reactions and $i$ species, the reaction rates $r_j$ (mol/m$^3$·s) can be described by the mass action law

$$r_j = k_j^f \prod_{i \in reactants} c_i^{-v_{ij}} - k_j^r \prod_{i \in products} c_i^{v_{ij}} \quad (7)$$

where $k_j^f$ and $k_j^r$ denote the forward and reverse constants, respectively. The concentration of species $i$ is denoted as $c_i$ (mol/m$^3$). The stoechiometric coefficients are denoted $v_{ij}$ and are defined as being negative for reactants and positive for products.

The rate of mole variation for a given specie integrates a contribution from each reaction in which the specie is involved, so that

$$R_i = \sum_j v_{ij} r_j \quad (8)$$

Furthermore, initial and boundary conditions must be written to solve the system.

The initial conditions apply

$$\rho_1^x(0) = 0 \quad (9)$$

$$\rho_2^x(0) = \rho_{20}^x \quad (10)$$

$$\rho_3^x(0) = \rho_{30}^x \quad (11)$$

$$\rho_4^x(0) = \rho_{40}^x \quad (12)$$

$$\rho_5^x(0) = \rho_{50}^x \quad (13)$$

$$\rho_6^x(0) = \rho_{60}^x \quad (14)$$

$$\rho_7^x(0) = 0 \quad (15)$$

The boundary conditions can be written as follows, assuming impermeable interface at the bottom of the domain ($x = 0$, solution/substrate interface), and liquid/vapor equilibrium at the upper interface, ($x = H_s$, solution/air interface)

$$\text{x} = 0, \qquad J_i = 0 \ \text{ for } i = 1 \text{ to } 7 \quad (16)$$

$$\text{x} = H_s, \qquad J_1 = k_1\left[\rho_1^e(T_b) - \rho_1^i(T)\right] \quad (17)$$

$$J_2 = k_2\left[\rho_2^e(T_b) - \rho_2^i(T)\right] \quad (18)$$

$$J_i = 0 \ \text{ for } i = 3 \text{ to } 7 \quad (19)$$

where $J_i$ (kg/m$^2$·s) is the flux of specie $i$, $k_1$ and $k_2$ (m/s) the ammonia and water external mass-transfer coefficients. $\rho_{i0}^x$ and $\rho_i^x(t)$ (kg/m$^3$) are the initial concentration and the concentration of $i$ in the polymeric system, respectively. $\rho_1^e$ and $\rho_2^e$ (kg/m$^3$) are the concentration of ammonia and water in the external phase (atmosphere). $\rho_1^e$ and $\rho_2^e$ depend on the bulk temperature. The concentration of these two species at the interface will be noted $\rho_1^i$ and $\rho_2^i$, respectively. $\rho_1^i$ and $\rho_2^i$ depend on the solution temperature. In Eq. 19, the acetic acid evaporation is neglected since its initial amount is very low and it is assumed to quickly react with ammonia. In addition, the concentrations of water and ammonia in the gas phase and at the interface can be expressed as follows

$$\rho_1^e = \frac{P_{sv1}(T_b) \times M_1}{RT} \quad (20)$$

$$\rho_1^i = \frac{P_{v1}(x_{1i}, T) \times M_1}{RT} \quad (21)$$

$$\rho_2^e = \frac{RH \times P_{sv2}(T_b) \times M_2}{RT} \quad (22)$$

$$\rho_2^i = \frac{P_{v2}(x_{2i}, T) \times M_2}{RT} \quad (23)$$

where, $P_{svi}$ $(T_b)$ is the external saturating vapor pressure of $i$, $M_i$ the molecular weight of $i$ (kg/mol), and $R$ (J/mol·K) the ideal gas constant.

### *Heat-transfer model*

During the gelation process, the temperature may change, mainly due to the water vaporization and ammonia absorption. Several parameters involved in the mass-transfer phenomena coupled to chemical reactions depend on the temperature among which the diffusion coefficients and the reaction kinetic constants. Hence, it is believed that a better modeling of the experimental data will be reached including a coupling between heat and mass transfers in the model. Since the Biot number was found to be lower than 0.01 for the numerical conditions ($3.3\ 10^{-3}$), uniform temperature was assumed throughout the polymeric system (basic assumption n°3). A lumped parameter approach was applied to predict the global heat transfer rate[41]

$$\frac{dT}{dt} = -\left[\frac{h_b^{\text{up}}(T - T_b) + h_b^{\text{down}}(T - T_b) + J_1\Delta H_{v1} + J_2\Delta H_{v2}}{\rho_s Cp_s H_s + \rho_g Cp_g H_g + \rho_{ss} Cp_{ss} H_{ss}}\right] \quad (24)$$

where $\rho$ (kg/m$^3$) and $Cp$ (J/kg·K) are the density and heat capacity, respectively. Subscripts $s$, $g$ and $ss$ refer to the polymeric solution, the glass substrate and the stainless steel plate, respectively. $\Delta H_{v1}$ and $\Delta H_{v2}$ (J/kg) are the heat of vaporization of ammonia and water, respectively. $T$ (K) is the temperature of the system, and $T_b$ (K) is the bulk temperature. $H_s$, $H_g$ and $H_{ss}$ (m) represent the solution, the glass Petri dish, and the stainless steel plate thicknesses, respectively.

### *Determination of mass and heat-transfer coefficients*

The mass-transfer coefficient for free convection of component $k_i$ can be determined from the empirical correlation given by Yip and McHugh[41]

$$\frac{k_i L_c y_{air,lm}}{M_i D_{i/g}} = 0.27(Gr\ Sc_i)^{0.25} \quad (25)$$

where $Gr$ is the Grashof number, $Sc_i$ is the Schmidt number related to $i$, $D_{i/g}$ (m$^2$/s) is the mutual diffusion coefficient of $i$ in the gas phase, $L_c$ (m) the characteristic length of the interface and $y_{air,lm}$ the log-mean mole fraction difference of air. The Schmidt number has its standard definition. It is the

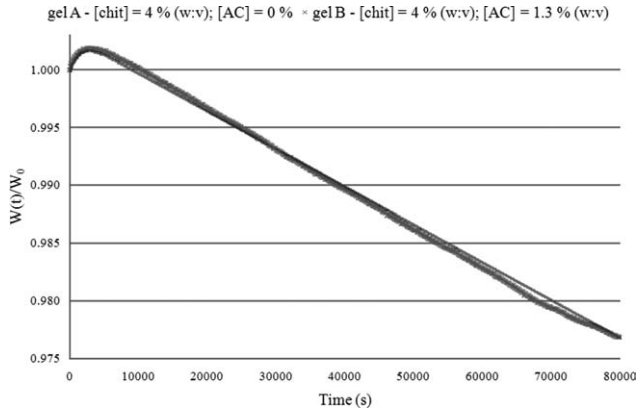


**Figure 4. Influence of AC on gravimetric kinetics.**

$W(t)$ = weight, and $W_0$ = initial weight. $[NH_3]_{solution} = 2\%$ (w:w); $T = 303$ K; $t_{VIPS} = 24$ h.

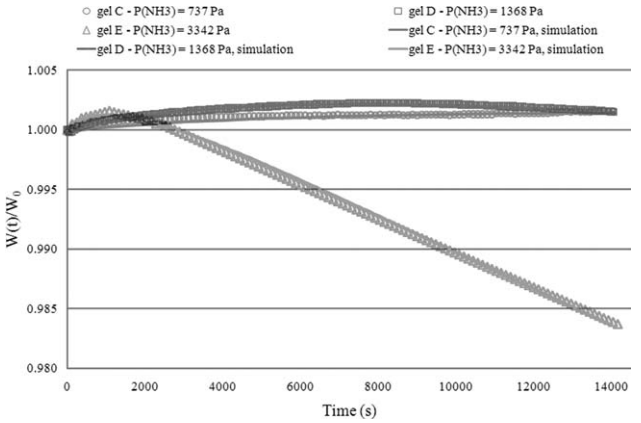


**Figure 5. Influence of nonsolvent partial pressure on gels gravimetric kinetics.**

$W(t)$ = weight; $W_0$ = initial weight, and $t_{VIPS} = 4$ h; [chitosan] = 3.25% (w:v).

ratio between the cinematic viscosity and the diffusion coefficient. The Grashof number incorporates both the temperature and the concentration effects on the variation in the gas-phase density.[51] It is expressed as following

$$Gr = \frac{L_c^3 g \rho_a}{\mu_a^2}\left| -\frac{1}{\rho_a} \times \left(\frac{\partial \rho_a}{\partial T}\right)_{P,y_i} \times (T - T_b) - \sum_i \left( -\frac{1}{\rho_a}\left(\frac{\partial \rho_a}{\partial y_i}\right)_{P,T} \times (y - y_i)\right)\right| \quad (26)$$

where $g$ (m/s$^2$) is the acceleration due to gravity, $\rho_a$ (kg/m$^3$) is the air density in the gas phase, and $\mu_a$ (Pa·s) is the dynamic viscosity of air.

The free convection heat-transfer coefficients for the different species are also determined using empirical correlations

$$\frac{hL_c}{\lambda_a} = 0.27(Gr\,Pr)^{0.25} \quad (27)$$

where $\lambda_a$ (W/m·K) is the thermal conductivity of air, and $Pr$ is the Prandtl number. This dimensionless number can also be calculated using its standard definition. It is the ratio between the kinematic viscosity and the thermal diffusivity.[51]

### *Numerical algorithm*

The coupled equations, corresponding to mass transport, heat transfers and chemical reactions, and the associated boundary conditions were solved numerically using finite element software: COMSOL Multiphysics. 3.5. Fine meshes could be employed, thanks to a fast resolution for unidirectional geometry. The mesh was, thus, refined in the zone of the gas/system interface, where the concentration gradients were expected to reach maximum values. In addition, a variable time step was used.

## Results and Discussion

### *Experimental results*

A global result can be given concerning the kinetic curves behaviors (Figures 4 to 6). Each gravimetric kinetic can be divided into two parts, each one corresponding at least to one specific phenomenon as previously observed when applying the VIPS process to other systems.[35]

As the chemical potential of $NH_3$ in the polymeric solution is assumed to be zero at the beginning of the experiment, there is an ammonia inflow into the liquid film resulting in a weight intake (Eq. 17). The ammonia reacts with the quaternium chitosan formed during the dissolution step, and then gelation occurs (Eq. 3). Ammonia keeps on transferring from the vapor phase to the gel phase until the ammonia chemical potentials in the gel and in the vapor phase become equal. The decreasing part of the curves corresponds to a water outflow (Eq. 18). The mass-transfer rate is also reduced compared to initial ammonia inflow since the water chemical potential gradient is lower.

### *Influence of AC on gravimetric study*

Figure 4 compares gravimetric curves obtained for a chitosan hydrogel and a composite chitosan-AC hydrogel. The only difference between both experiments corresponds to the

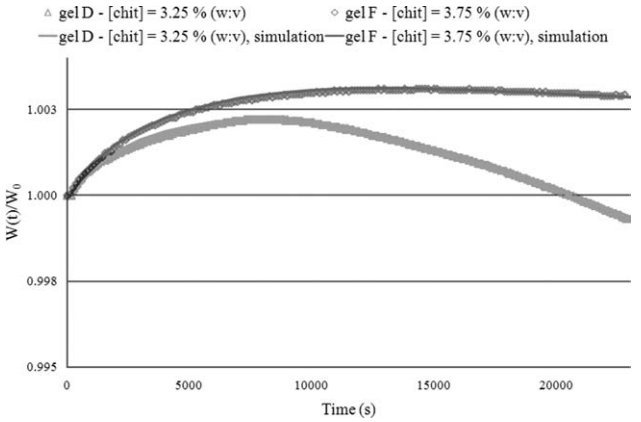


**Figure 6. Influence of chitosan concentration on gels gravimetric kinetics.**

$W(t)$ = weight; $W_0$ = initial weight, and $t_{VIPS} = 6.5$ h; $P_{NH3} = 1368$ Pa.

AC amount, all the other parameters, i.e., the initial chitosan concentration, the bulk temperature, the ammonia concentration in the solution and the exposure time to the nonsolvent vapors, being the same.

This result clearly shows that AC does not influence the global mass exchanges during the gel formation. As a matter of fact, the consistence of the basic assumption considering that AC does not play any major role on the whole gelation process is proved. However, if AC had more surface acidic functions, then it might be possible to notice a difference in terms of ammonia intake because these functions would be neutralized by the basic vapors used to induce the gelation. Thus, the ammonia gradient should be slightly higher in the case of the composite gel, leading to a different kinetic curve.

### *Influence of nonsolvent partial pressure ($P_{NH3}$) on gravimetric curves*

Three different partial pressures were tested: 737, 1368 and 3342 Pa (Figure 5). To create the ammonia vapors, the ammonia concentration in the liquid bath ranged from 0.875% to 1.625% in weight. These values are in the same order of magnitude as those reported in previous work using ammonia to induce gelation.[27]

The ammonia partial pressure plays a key role on the time needed to induce a complete gelation. For the lowest value of the partial pressure (737 Pa), the weight of the matrix keeps on increasing during the whole experiment. When this pressure is set to 1368 Pa, a maximum is reached after 2 h (7,200 s), and then, the weight of the system slowly decreases. Finally, for the highest ammonia partial pressure (3342 Pa), the matrix weight quickly increases, and a maximum is reached after only 10 min (600 s), then, the global mass decreases until the end of the process.

These gravimetric curves highlight the influence of the nonsolvent partial pressure, which controls the driving force, as well explained by Caquineau et al. who studied the influence of the relative humidity in porous membrane formation using the poly(ether imide)/*N*-methyl-2-pyrolidone/water system.[33] In their work, water was the nonsolvent. They exhibited different gravimetric behaviors when RH value was increased. Furthermore, different gravimetric kinetics under different RH were also reported in another study dealing with membrane formation by VIPS process and using another system (polysulfone/*N*-methyl-2-pyrolidone/water).[52]

In this work, the maximum sample weight is reached earlier when increasing the ammonia partial pressure since the ammonia concentration gradient between the gas phase and the air/solution interface is higher. As a result, the driving force for mass transfers is higher leading to higher mass-transfer rates during the first minutes. In addition, the maximum value reached in each case is in the same order of magnitude ($w(t)/w_0 = 1.0025$). It can be explained by the fact the initial polymer amount is the same for each experiment. It means that the number of protonated sites on chitosan which are involved in the chemical reaction with ammonia is the same. In addition, *AcOH* remaining from the equilibrium reaction of chitosan solubilization is the same too.

### *Influence of chitosan concentration on gravimetric curves*

The goal of this experiment was to investigate whether the polymer concentration could significantly influence the gravimetric kinetics. The choice of the concentration range was made from previous experiments. With this specific chitosan batch (342), gels prepared by the VIPS process with a 3% w:v concentration lead to breakable composites, whereas for polymer concentration higher than 4% (w:v), the solutions were too viscous to allow their homogeneous casting. Thus, it was decided to prepare gels with two intermediary concentrations: 3.25 $\pm$ 0.01% and 3.75 $\pm$ 0.01% (w:v).

An increase of the chitosan concentration is expected to increase the maximum weight intake since more sites are available to react with ammonia leading also to higher ammonia intake. Figure 6 presents the two gravimetric kinetics obtained for the two different initial chitosan concentrations: 3.25 $\pm$ 0.01% and 3.75 $\pm$ 0.01% (w:v). In terms of protonated sites, these concentrations correspond, respectively, to the following values: 1.49 $10^{-1}$ $mol_{Chit\text{-}NH3+}$/L and 1.71 $10^{-1}$ $mol_{Chit\text{-}NH3+}$/L. A slight difference in terms of weight intakes is observed: the maximum $w(t)/w_0$ values are 1.0022 $\pm$ 0.0001 and 1.0031 $\pm$ 0.0001, reached after 2.2 h (7,920 s) and 3.5 h (12,600 s), respectively. The maximum of the curve is reached earlier for the lowest polymer concentration, as expected, since the amount of protonated sites was decreased at lower polymer concentration.

Thus, this parameter slightly affects the gravimetric kinetics during the gel formation. Moreover, the chitosan concentration has an effect on the interactions between the intermolecular chains, since at higher polymer concentrations the junctions between the polymer chains will be enhanced. It could also control the final morphology of the hydrogels. Indeed, as reported in a study on the polysulfone/*N*-methyl-2-pyrolidone/water system, it was shown that the pore sizes were strongly affected by the concentration of the initial polymer solution.[37] When the polymer concentration is higher, the polymer solution viscosity is higher too and, thereby, the mobility of the polymer chains is reduced.

### *Simulation results*

An appropriate usual method to follow gelation of chitosan matrices is rheology. A continuous measurement of both the storage modulus and the loss modulus during the gelation process permits to define the gel point by plotting the two moduli at one specific frequency over time.[31] Such a method is very useful to follow the gelation, from a mechanical point of view, since as soon as the storage modulus becomes higher than the loss modulus, elastic properties responsible for the gel behavior dominate. Then, it is convenient to study the influence on the gelation kinetics of different parameters such as the degree of acetylation or the polymer concentration. In this case, the gelation is induced by a pH change due to ammonia intake into the chitosan solution, and its diffusion toward the bottom of the sample. Locally in the chitosan solution, as soon as the pH becomes high enough, the protonated sites of the chitosan chains react with ammonia leading to the gelation. This phenomenon is expected to occur quasi immediately after the contact with

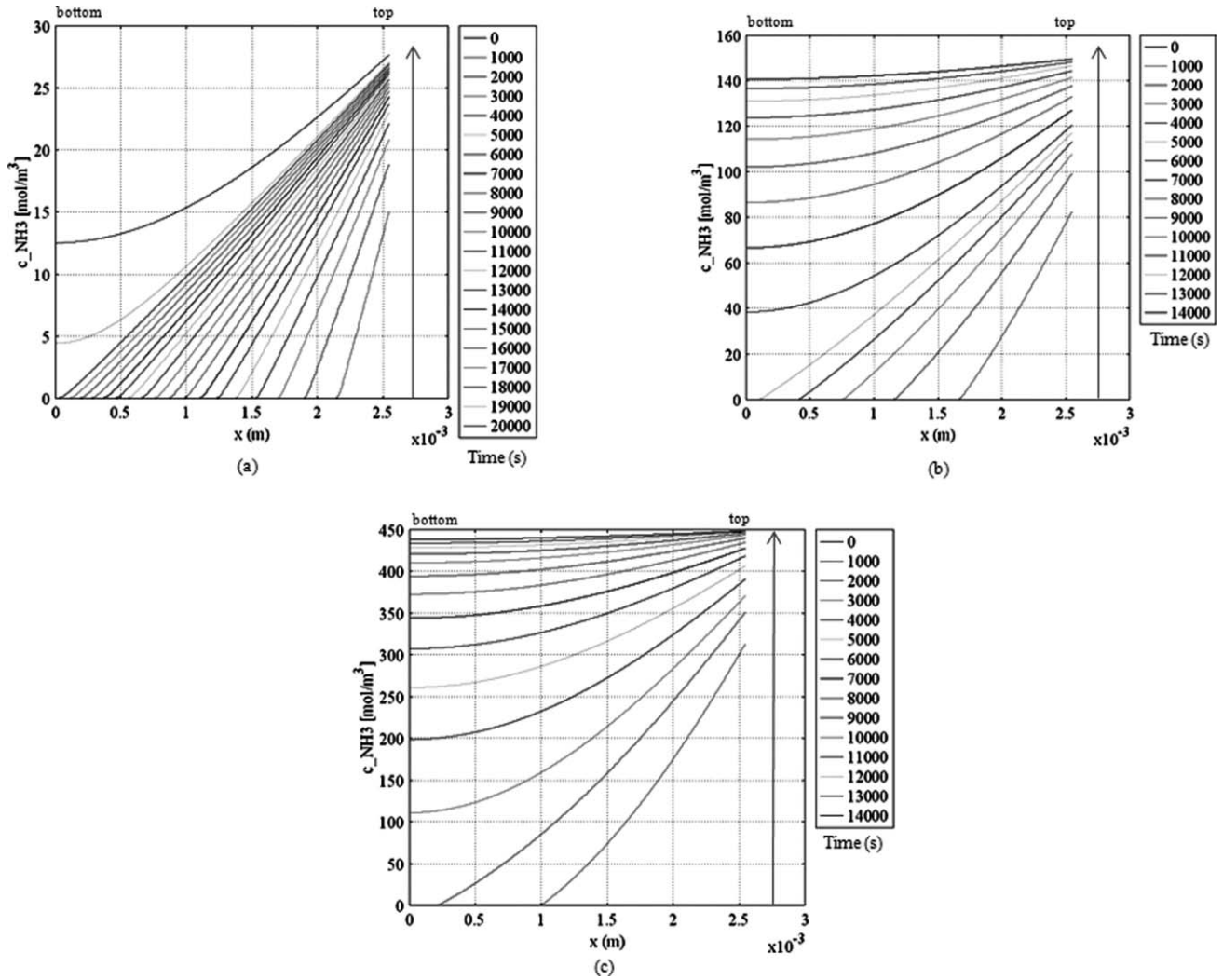


**Figure 7. Ammonia concentration profiles.**

(a) $P_{NH3}$ = 737 Pa; [chitosan] = 3.25% (w:v), (b) $P_{NH3}$ = 1368 Pa; [chitosan] = 3.25% (w:v), and (c) $P_{NH3}$ = 3342 Pa; [chitosan] = 3.25% (w:v).

the basic media. Indeed, no delay time is expected in the gelation process as reported when a chitosan solution is added dropwise to a basic coagulation liquid.[53,54] Thus, the knowledge of the equilibrium constant of the chemical reaction involving $Chit\text{-}NH_3^+$ and $NH_3$, and the prediction of the pH variation inside the solution during the process can be used in a first approach to predict the moving rate of the gelation front.

In this section, the results concerning the mass-transfer simulations are presented in order to discriminate the main phenomena involved in gelation. A better understanding of transfers responsible for the final hydrogel morphology is also expected by analyzing the concentration profiles of all species.

### *Gravimetric kinetics*

Three main parameters control the external transfers, for a given chitosan concentration: the ammonia partial pressure in the atmosphere, the external mass-transfer coefficients and the relative humidity. The ammonia partial pressure in the gas phase above the system controls the ammonia transfer between the atmosphere and the gas/solution interface, whereas RH controls the water exchanges between the atmosphere and the solution. For one specific experiment, all parameters are known from the operating conditions, the literature or directly calculated with the model. However, the value of the relative humidity is more difficult to estimate with enough accuracy by experimental method. Actually, this parameter was experimentally estimated with a probe with a 1% experimental error. Besides, the RH value is expected to control the water transfer rate (by evaporation) that is mainly visible in the second part of the gravimetric curve, after the ammonia intake. During this second step characterized by a constant drying period, the curve has a linear trend. Since the sensibility of the slope to the RH value is very high, the relative humidity will be used in the numerical model to fit the decreasing part of the gravimetric curves.

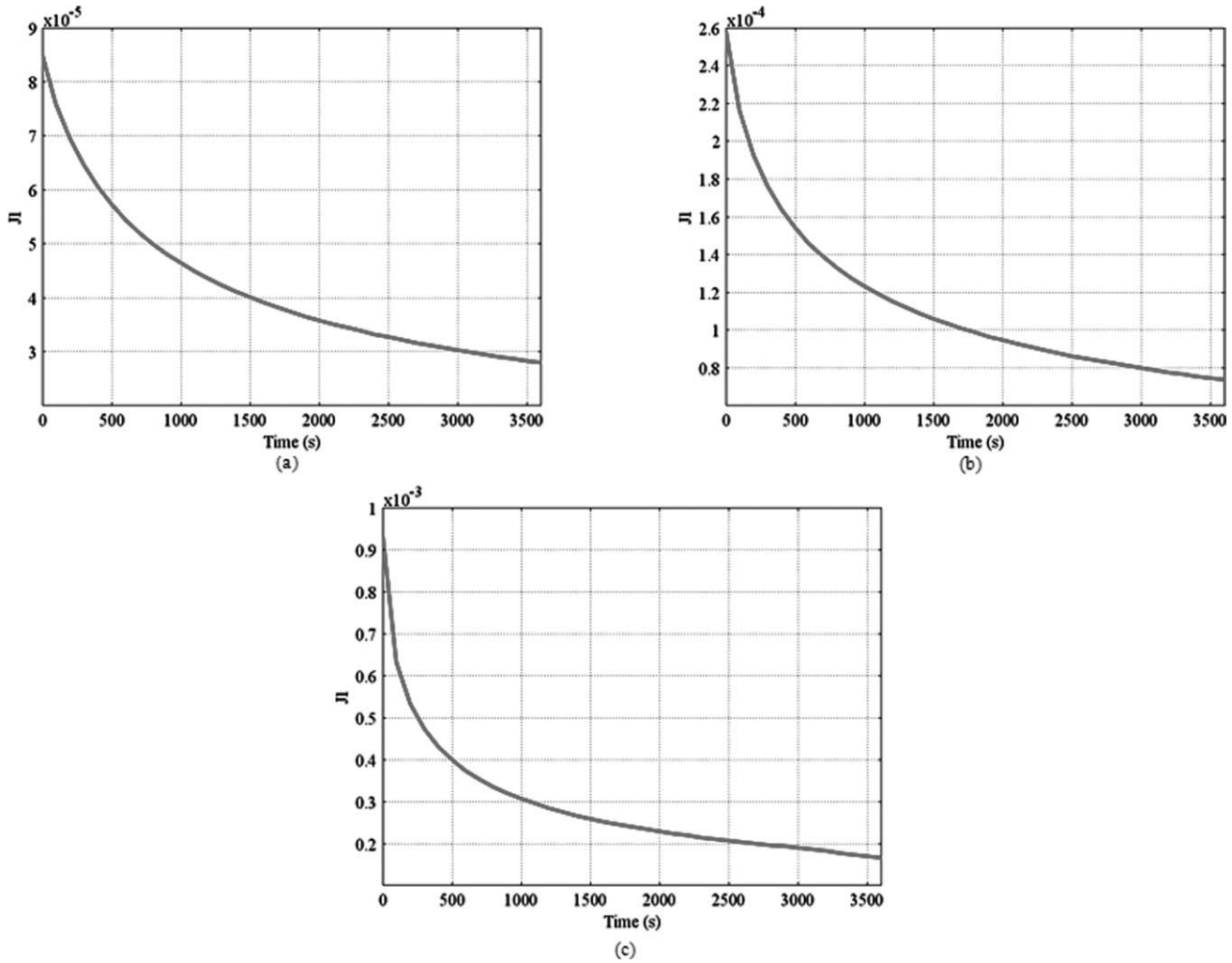


**Figure 8. Ammonia fluxes.**

(a) $P_{NH3}$ = 737 Pa; [chitosan] = 3.25% (w:v), (b) $P_{NH3}$ = 1368 Pa; [chitosan] = 3.25% (w:v), and (c) $P_{NH3}$ = 3342 Pa; [chitosan] = 3.25% (w:v).

Although a slight difference is observed between experimental and simulated data, the model gives accurate predictions comparing to experimental results as shown in Figures 5 and 6.

Thus, the initial assumption considering that only water and ammonia are involved in external mass transfers is relevant (Eqs. 17 and 18). However, because (1) the initial RH was high (more than 96%), and (2) water is the main component of the system (>96% in weight), it was previously expected that the water chemical potential difference would be low, inducing rather low-water concentration gradients. Thus, the analysis of ammonia concentration gradients should be more helpful for a better understanding of transfers.

Since both experimental and numerical data are in fairly good agreement, the numerical model could be used to go beyond in the analysis. Gravimetric kinetics only represents the global result of the local transfers and chemical reactions phenomena involved in the gelation. Therefore, concentration profiles were predicted vs. time using the model in order to precise the local mass transfers involved for the different parts of the kinetic curves.

### *Ammonia concentration profiles*

Figure 7 presents the ammonia concentration profiles over time for different ammonia partial pressures in the atmosphere above the system. Whereas for $P_{NH3}$ = 1,368 Pa (Figure 7b), and $P_{NH3}$ = 3342 Pa (Figure 7c), ammonia is available at the bottom of the film ($x = 0$) after less than 2,600 s (43 min), and about 5,000 s (1 h 23 min), respectively, this is not the case for $P_{NH3}$ = 737 Pa (Figure 7a). For this specific operating condition, ammonia reaches the bottom of the film after 18,000 s (5 h). High-initial ammonia partial pressures induce high-transfer rates and so, high-initial ammonia gradients. As a result, ammonia is quickly available in the whole system thickness to react with chitosan. On the contrary, for low-ammonia partial pressure, low-concentration gradients are responsible for the delay in the ammonia penetration deeper in the chitosan solution. This

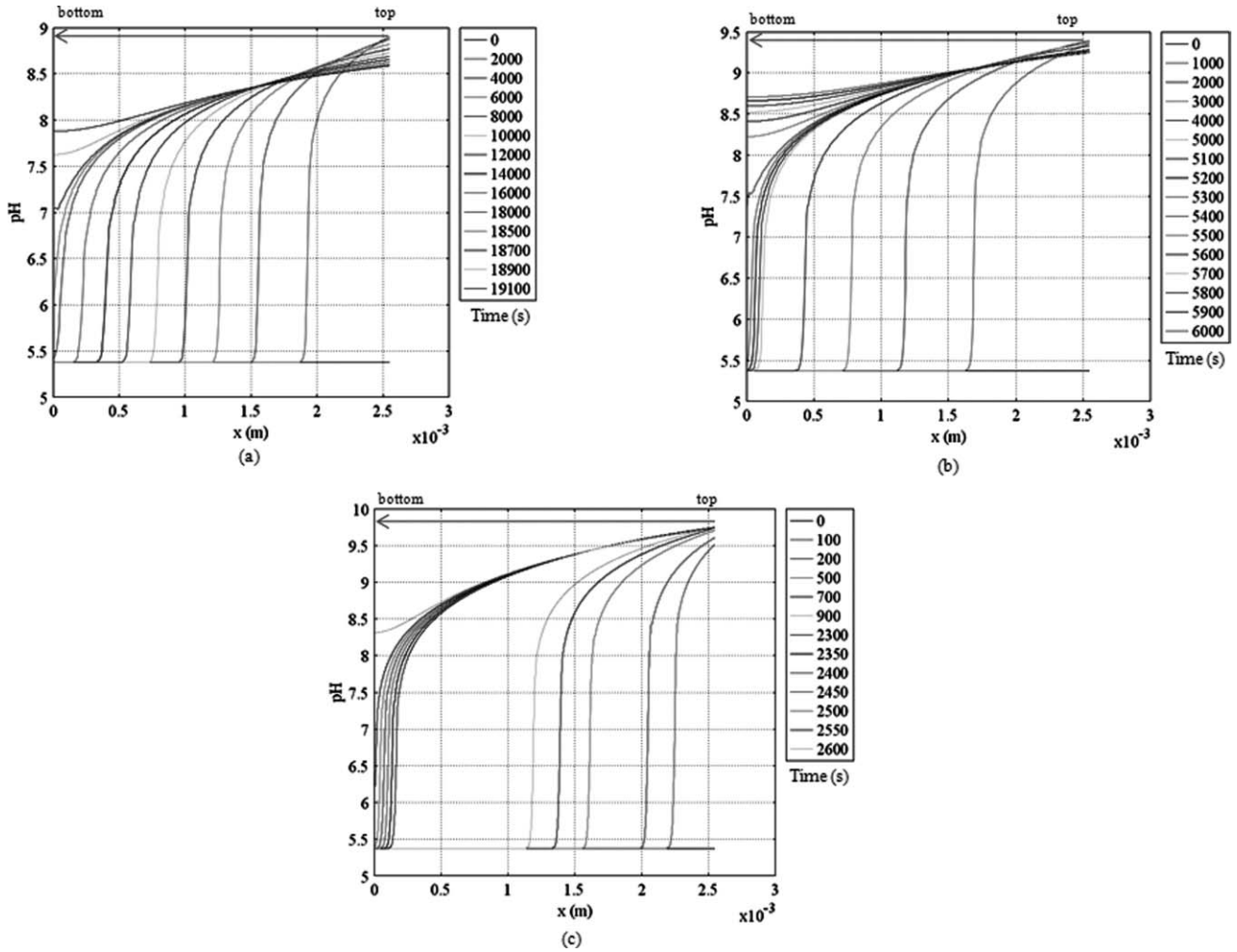


**Figure 9. pH profiles.**

(a) $P_{NH3}$ = 737 Pa; [chitosan] = 3.25% (w:v), (b) $P_{NH3}$ = 1368 Pa; [chitosan] = 3.25% (w:v), and (c) $P_{NH3}$ = 3342 Pa; [chitosan] = 3.25% (w:v).

difference in terms of ammonia availability is also put in evidence in Figure 8, which reports the ammonia fluxes ($J_1$) during the first hour of the gelation process. It is confirmed that (1) gelation is induced by an ammonia inflow, and (2) the ammonia amount transferred from the gas/solution interface to the solution depends on the initial ammonia partial pressure, which is also expected to control the time to reach a complete gelation in the system. In addition, Figure 7 shows that the ammonia transfer mostly happens in the first three hours ($t < 10{,}800$ s) for nonsolvent partial pressure >1368 Pa with strong concentration gradients in the first hour. Then, the profiles tend to be flat indicating that the concentration gradients decrease between the chitosan solution and the gas phase.

### *pH profiles*

Another way to follow the gelation and to predict the minimum gelation time is to investigate the progression of the pH front in the polymeric system. Throughout the process, a change of pH happens linked to ammonia diffusion and chemical reactions occurring in the system. Thus at time $t$, the value of the pH depends on the location in the system.

When ammonia transfers from the vapor phase to the matrix (Eq. 17), the pH increases because of the dissociation of ammonia in aqueous phase, described by the following equation

$$NH_3 + H_2O \Leftrightarrow NH_4^+ + OH^- \tag{28}$$

where $OH^-$ represent the hydroxide ions.

A pH variation is responsible for the gelation process as explained in literature.[53,55,56] Thus, measuring the pH or simulating these data is also a convenient method to follow the gelation kinetics. Figure 9 presents the pH profiles obtained for different ammonia partial pressures. At the beginning, the pH is low (<5.5) because chitosan is under soluble form, since acidic aqueous media (*AcOH*) was initially added to protonate chitosan amino groups (Eq. 1). It was previously shown that when adding a strong base to a chitosan solution, chitosan remains in soluble state up to a pH in the vicinity of 6.2. However, further basification (pH > 6.2) systematically led to the formation of a hydrated

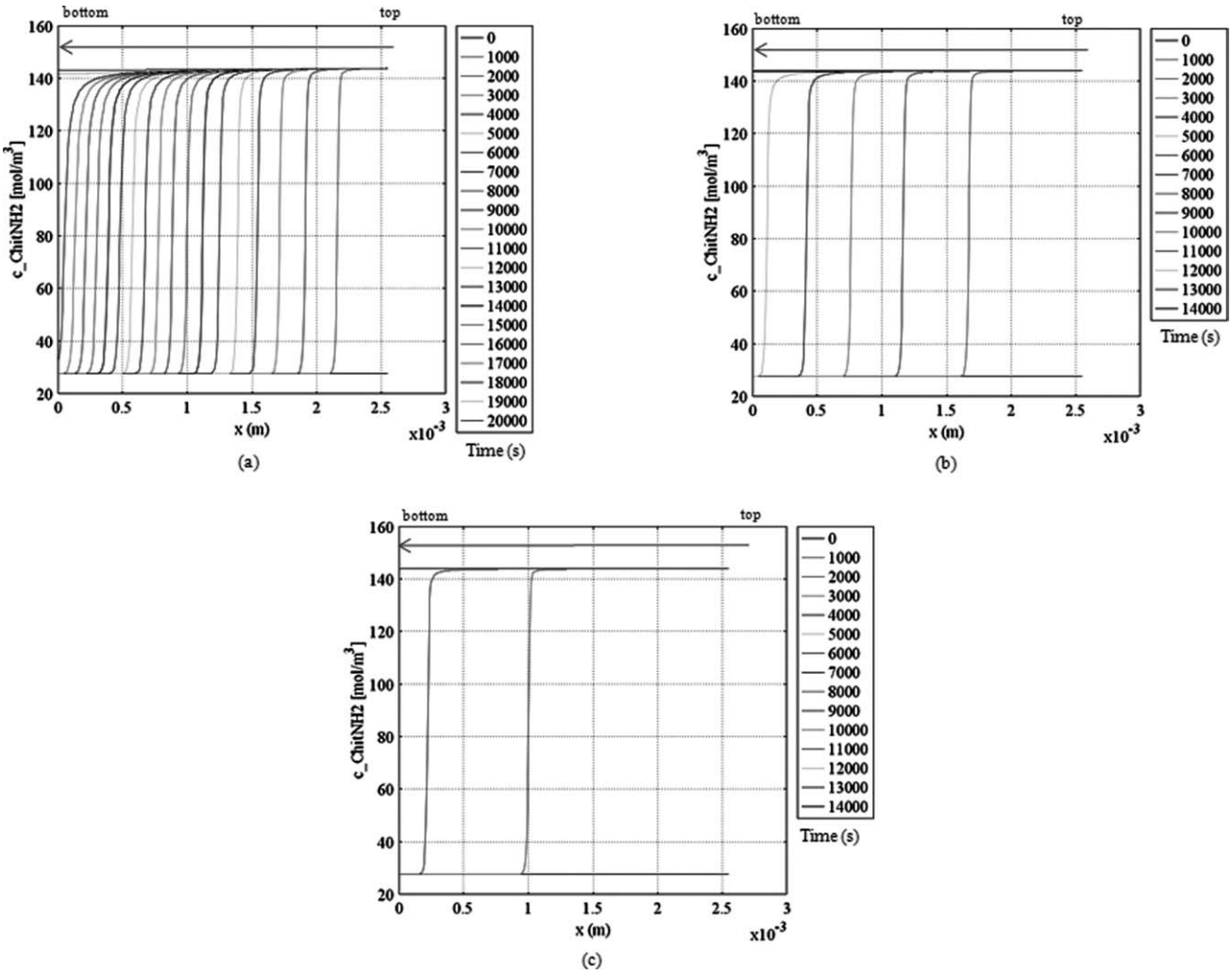


**Figure 10. *Chit-$NH_2$* concentration profiles.**

(a) $P_{NH3}$ = 737 Pa; [chitosan] = 3.25% (w:v), (b) $P_{NH3}$ = 1368 Pa; [chitosan] = 3.25% (w:v), and (c) $P_{NH3}$ = 3342 Pa; [chitosan] = 3.25% (w:v).

gel-like precipitate.[56] The precipitation or gel formation was due to the neutralization of chitosan amine groups (Eq. 3), and the consequent removal of repulsive interchain electrostatic forces which subsequently allowed for extensive hydrogen bonding and hydrophobic interactions between chains.

From these considerations, gelation can be reached in the whole matrix as soon as pH > $pK_a$. However, no exact value, as far as we know, is reported in the literature because it depends on the chitosan properties such as its DA.[1] The chitosan dissociation degree also influences the $pK_a$ since values ranging from 6.1 to 6.7 for different dissociation degrees are reported.[57] Considering data available in literature, $pK_a$ = 6.4 was chosen in this study. The pH profiles are, thus, helpful for a better approach of the gelation time since it is considered that the gel is totally formed when pH > $pK_a$ in the whole thickness of the matrix. For $P_{NH3}$ = 737 Pa (Figure 9a), pH becomes higher than the critical value in the full thickness after 18,500 s (5.1 h). For $P_{NH3}$ = 1368 Pa (Figure 9b), pH = $pK_a$ for an exposure time to vapors ranging from 5,300 s to 5,400 s (1.5 h), whereas less than 2,600 s (43 min) are required to complete the gelation when $P_{NH3}$ is increased to 3342 Pa (Figure 9c). These results can be compared to previous conclusions concerning the ammonia concentration profiles. In each case, the duration required to reach the gelation pH in the whole system is in the same order of magnitude of the time required by ammonia to reach the bottom of the system. Thus, it confirms the fact that the chemical reaction kinetics are not the limiting step of the process since as soon as ammonia is in contact with the acidic species (*AcOH* and *Chit-$NH_3^+$*), neutralization occurs leading to a fast increase of pH value.

### *Chitosan concentration profiles*

Figure 10 presents the concentration profiles of *Chit-$NH_2$*. Since the chemical reactions are clearly not the limiting step of the process, as soon as the different species come into contact, meaning as soon as ammonia transfers from the gas-liquid interface to the liquid, proton exchanges happen very quickly between the acid, *Chit-$NH_3^+$*, and the base, *$NH_3$*.[49] The result is the formation of their conjugated species,

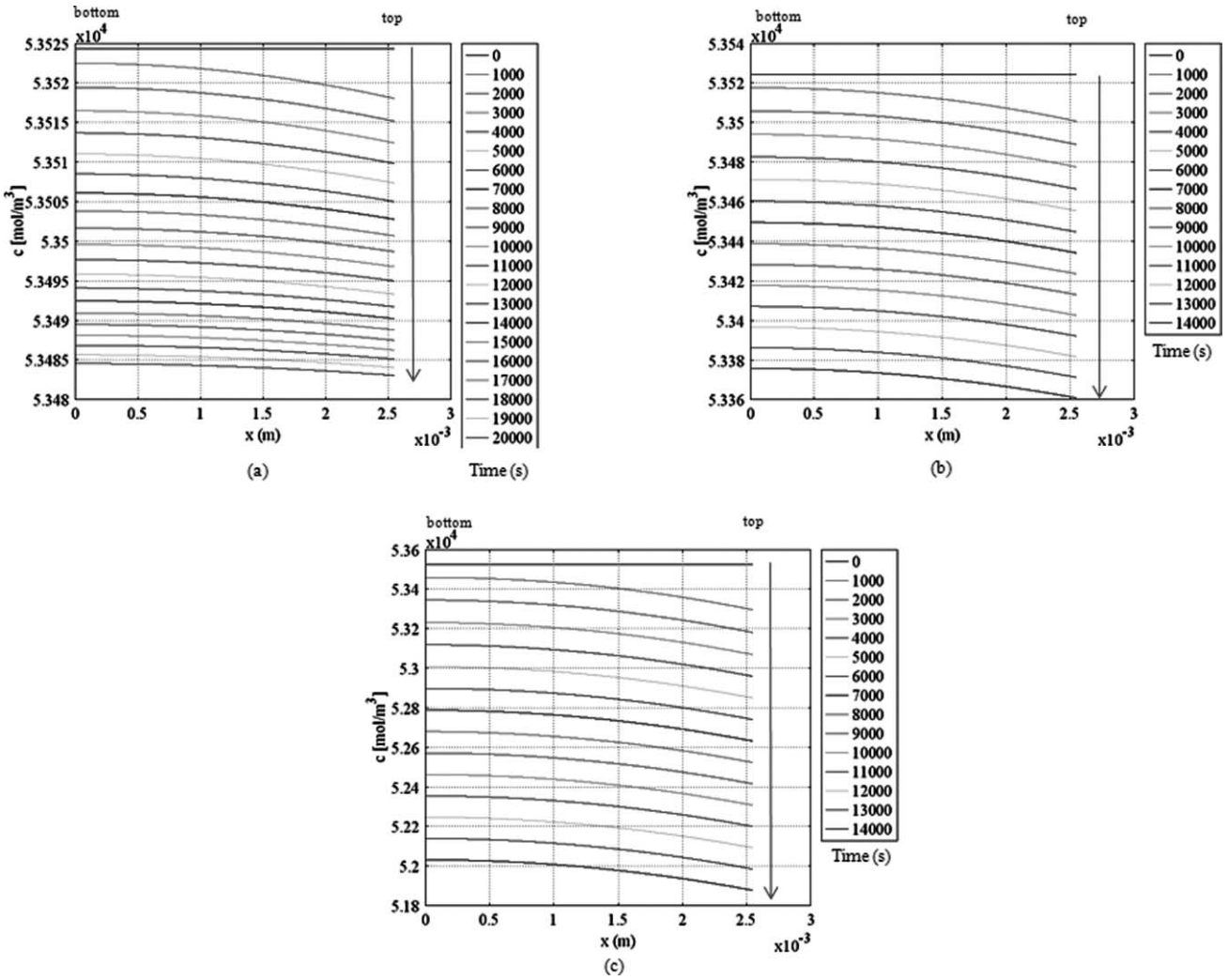


**Figure 11. Water concentration profiles.**

(a) $P_{NH3}$ = 737 Pa; [chitosan] = 3.25% (w:v), (b) $P_{NH3}$ = 1368 Pa; [chitosan] = 3.25% (w:v), and (c) $P_{NH3}$ = 3342 Pa; [chitosan] = 3.25% (w:v).

*Chit-NH*$_2$ and $NH_4^+$, respectively. The higher $P_{NH3}$, the faster these concentration fronts will move from the top to the bottom of the sample. Thus, for the highest value ($P_{NH3}$ = 3342 Pa), *Chit-NH*$_2$ is present in the whole film thickness in less than 3,000 s (Figure 10c) whereas for $P_{NH3}$ = 737 Pa, almost 18,000 s are required (Figure 10a).

Whatever the operating conditions, the gelation will start at the top of the sample. The lifetime of this biphasic system (gel and liquid) depends on $P_{NH3}$, because it controls the ammonia transfer driving force. For hybrid process involving simultaneously VIPS and wet process, different authors have shown that the exposure time to nonsolvent vapors is a crucial factor influencing the final films morphology.[32,35] Thus, different cellular structures have been obtained for different exposure time to nonsolvent vapors. Although the works reported in the literature mainly concerned phase inversion mechanism, it is expected that the exposure time could have a significant effect on the final gel properties if the sample was immersed into a pure water bath too early. Indeed, the immersion should be done once the gelation is finished along the whole thickness of the sample. It is also very important to develop experimental or numerical tools in order to estimate this gelation time, and then the exposure time to the nonsolvent vapors.

### *Water concentration profiles*

Concerning the water concentration profiles, Figures 11 and 12 confirm that water evaporates from the matrix for all operating conditions. The concentration gradient is at maximum at the beginning of the process. It means that in the first part of gravimetric kinetics (Figures 4–6), a water outflow and an ammonia inflow happen simultaneously. The ammonia inflow is the predominant phenomenon during this initial period, resulting in a global system weight increase. No major difference is observed when the nonsolvent partial pressure increased. Globally, the low-water chemical potentials difference between the gas phase and the solution is the same. Therefore, the model input values were almost the same too, resulting in similar water concentration profiles,

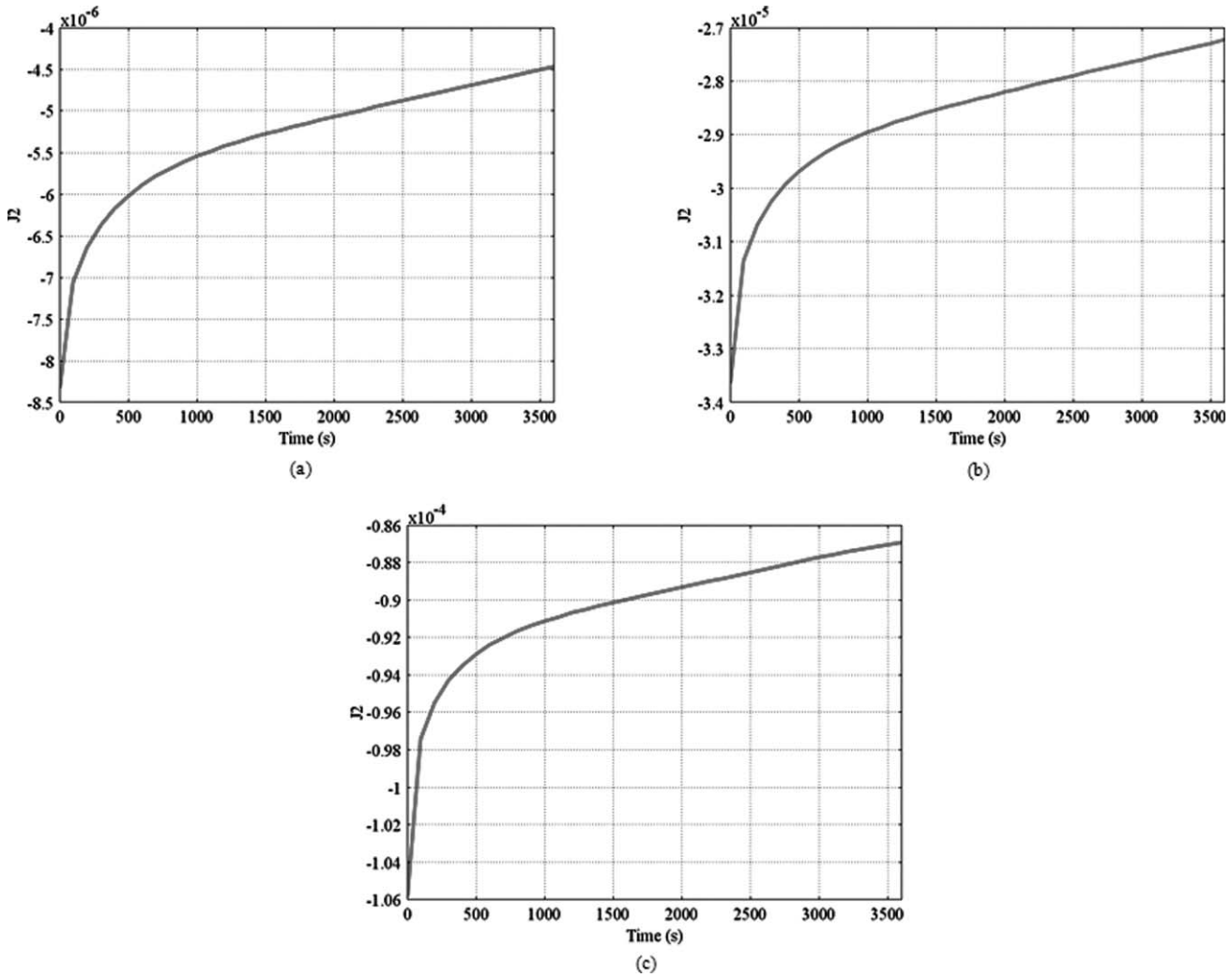


**Figure 12. Water fluxes.**

(a) $P_{NH3}$ = 737 Pa; [chitosan] = 3.25% (w:v), (b) $P_{NH3}$ = 1368 Pa; [chitosan] = 3.25% (w:v), and (c) $P_{NH3}$ = 3342 Pa; [chitosan] = 3.25% (w:v).

almost flat. Because water concentration profiles are very similar whatever the operating conditions, they can be neglected in the whole matrix structuring. Besides, the very low-evaporation rate of water will be assimilated to a drying step in smooth conditions. However, despite low-transfer rate, the water evaporation is responsible for heat transfer since its vaporization enthalpy, $\Delta H_{v2}$, is almost twice the heat of condensation of ammonia, $\Delta H_{v1}$ ($\Delta H_{v1}$ = 23 310 J/mol and $\Delta H_{v2}$ = 40 608 J/mol).

### *Discussion about the concentration profiles and the pH front*

The results concerning the concentration profiles can be useful to go further in the explanation of the matrix formation since the presence of local concentration gradients should be linked to the final gel morphology. Previous work insisted on the fact that the mechanisms for the symmetric morphology formation was difficult to explain. Such studies have linked the symmetrical morphology to the flat concentration profiles of the components involved in the film elaboration.[37] Concerning the wet process, fast exchanges between solvent and nonsolvent are assumed to be responsible for the macrovoïds formation, which are not acceptable for wound dressings. Thereby, such exchanges lead to the formation of a polymer concentrated region near the interface between the solvent and nonsolvent leading to the formation of a dense layer.[52] Using the vapor induced phase separation process, the mass-transfer rates are reduced, especially for the solvent extraction when a solvent with low volatility is chosen. In this work, the gelation process is induced by ammonia vapors, and the most important parameter is the ammonia diffusion rate within the chitosan solution. A symmetric morphology could be expected if the ammonia diffusion rate would be slow enough to allow the gelation to occur in the same conditions in the whole sample thickness. The ammonia concentration profiles (Figure 7) and the moving rate of pH front (Figure 9) clearly indicated that the mass-transfer rate were slow, whatever the ammonia partial pressure. These results confirm that symmetric morphologies and regular structures can be expected for the final chitosan gels when

using the VIPS-gelation process. Such results are in agreement with previous works dealing with the VIPS process for polymeric membrane formation, even though the elementary mechanisms are weakly different, involving no chemical reaction and phase inversion rather than gelation.[35,37]

One of the major interests of this modeling approach is to reach data that would be very difficult to get by experimental methods. Indeed, the VIPS-gelation process was shown to reduce the mass-transfer rates, leading to symmetric gel structures, but after the exposure to ammonia vapors, the chitosan gels are washed in water bath before use. If the wet process induces a very fast gelation after immersion in the ammonia bath, the VIPS-gelation process permits to delay the gelation in the whole sample. It is also necessary to control the duration of the VIPS stage before the following washing stage. Modeling the moving rate of the pH front helps quantifying this gelation time, and the whole process can be optimized.

Actually, for a low-ammonia partial pressure, Figures 7a, 9a and 10a point out that ammonia is available in the whole film thickness after almost 18,000 s (5 h), whereas the gel is expected to be formed earlier at the top surface. Such a delay is not expected to modify the final gel morphology, but it is crucial to quantify it with a fairly good precision. For higher ammonia partial pressures (3342 Pa), the time to reach complete gelation in the whole thickness is strongly reduced (<43 min).

Furthermore, a drying of the gel simultaneously occurs since the chemical potential of water is weakly higher in the gel than in the air. However, due to the very high RH in the chamber, this drying stage is performed in very smooth conditions and is also not expected to disturb the gel properties, even if the VIPS-gelation process is long (24 h). This was confirmed by the water concentration profiles predicted by the model (Figure 11), which exhibited very weak concentration gradients along the sample thickness.

Thus, this new work highlights the complexity to link the concentration profiles to the final structure in a system involving chemical reactions leading to gelation, since nothing is reported in the literature on the VIPS process applied to gelation. In other classical systems, concentration fronts would permit to conclude on the formation of asymmetric porous structure. In this specific system, rapid reactions lead to fast gelation once the ammonia comes into contact with the protonated sites of the chitosan chains. A gelation process controlled by slow mass transfers should also lead to symmetric structures. Thus, intensive characterization studies will have to be linked to the simulation results to complete this work.

## Conclusions

The understanding of the gel formation and the control of the final porous structure using the VIPS process and the modeling tools represent a great challenge. Although the process is known and the materials, chitosan gels and AC, are widely used, the VIPS process applied to gelation had never been done before.

In this work, the formation of chitosan-activated carbon composite hydrogels by VIPS process was studied throughout the gelation, using inline gravimetric measurements.

Whatever the operating conditions, the same gravimetric behavior was observed. In first part, global increasing of the system weight occurred, due to an ammonia inflow. It was followed by a weight loss which was the consequence of water evaporation.

Different results could be highlighted:

1. The AC particles used do not influence the gravimetric kinetics.

2. The ammonia partial pressure plays a key role on the gravimetric behaviors since its increase results in decreasing the time required to reach the maximum system weight. Gelation time is, as a consequence, lower.

3. Increasing the polymeric concentration results in increasing the protonated functions to be neutralized by the ammonia. Thus, the ammonia intake during gelation is higher at higher polymer concentration.

A nonisotherm mass-transfer model coupled to chemical reactions was proposed assuming Fickian diffusion and no chitosan nor AC influence on the water and the ammonia activity. It exhibited fairly good agreement with the experimental data obtained inline in the fabrication chamber. The numerical model permitted to predict the concentration profiles of all species. Strong concentration gradients were predicted for ammonia because it transferred slowly from the top to the bottom of the matrix. The ammonia transfer induced a rise of the pH, which permitted chitosan to turn from soluble ($Chit\text{-}NH_3^+$) to insoluble form ($Chit\text{-}NH_2$), and, thus, gelation to occur. The $Chit\text{-}NH_2$ concentration profiles were very pronounced too, leading to concentration fronts. The water concentration profiles were almost flat whatever the ammonia partial pressure and the RH value because of very low-chemical potential difference between the gas phase and the solution. Following the pH moving front along the film thickness allowed predicting the gelation time in different conditions. This is crucial for the whole process since the hydrogel is washed into a water bath after being exposed to ammonia vapors. The gelation time was shown to be reduced when the ammonia vapor pressure was increased.

Further works are being performed concerning the characterization of the porous structure by ESEM changing the operatory conditions. To make it possible, hydrogels will have to be previously dehydrated with a process allowing a low shrinkage and as a consequence a low destructuring. Simulation should be linked to ESEM observations. If observations of gels prepared under low-ammonia partial pressure conditions show a global symmetric structure, as expected, then the composites will form the porous layer in contact with the wound and another layer, made of a dense structure will have to be applied above it. Thanks to the conclusion given by this study, all these works put together should lead to the optimization of the operating conditions to obtain a suitable hydrogel for the targeted application.

## Notation

$c_i$ = concentration of $I$, mol/m$^3$
$Cp_g$ = heat capacity of glass, J/kg·K
$Cp_s$ = heat capacity of the polymeric solution, J/kg·K
$Cp_{ss}$ = heat capacity of inox, J/kg·K
$D_{i/g}$ = mutual diffusion coefficient of $i$ in the gas phase, m$^2$/s
$D_{i/m}$ = mutual diffusion coefficient of $i$ within the matrix, m$^2$/s

$g$ = acceleration due to gravity, m/s$^2$
$Gr$ = Grashof number
$h$ = heat-transfer coefficient, W/m$^2$·K
$h_b^{up}$ = heat-transfer coefficient at the air side, W/m$^2$·K
$h_b^{down}$ = heat-transfer coefficient at the bottom of the system, W/m$^2$·K
$H_g$ = glass Petri dish thickness, m
$H_s$ = polymeric system thickness, m
$H_{ss}$ = stainless steel plate thickness, m
$\Delta H_{vi}$ = heat of vaporization of $i$, J/kg
$J_i$ = mass flux of $i$, kg/m$^2$·s
$k_i$ = mass-transfer coefficient of $i$ for free convection, s/m
$k_j^f$ = forward rate constant of reaction $j$ (its units depend on the order of the reaction)
$k_j^r$ = reverse rate constant of reaction $j$ (its units depend on the order of the reaction)
$K_{a,(AH/A-)}$ = acid/base equilibrium constant between $AH$ and its conjugate form $A^-$
$L_c$ = characteristic length of the interface, m
$M_i$ = molecular weight of $i$, kg/mol
$Pr$ = Prandtl number
$P_{svi}$ = saturating vapor pressure of $i$, Pa
$P_{vi}$ = vapor pressure of $i$, Pa
$r_j$ = reaction rate of $j$, mol/m$^3$·s
$R$ = ideal gas constant, J/mol·K
$R_i$ = rate expression for a given specie $i$, its units depend on the orders of the reactions in which $i$ is involved
$RH$ = relative humidity in the atmosphere in the reactor, %
$Sc_i$ = Schmidt number
$T_b$ = temperature of the bulk, K
$y_{air,lm}$ = log-mean mole fraction difference of air
$\lambda_a$ = thermal conductivity of air, W/m·K
$v_{ij}$ = stoechiometric coefficient of specie $i$ in reaction $j$
$\rho_a$ = air density, kg/m$^3$
$\rho_g$ = density of the glass Petri dish, kg/m$^3$
$\rho_s$ = density of the solution, kg/m$^3$
$\rho_{ss}$ = density of the stainless steal plate, kg/m$^3$
$\rho_i^x(t)$ = concentration of $i$, kg/m$^3$
$\rho_{i0}^x$ = initial concentration of $i$, kg/m$^3$
$\rho_i^e$ = concentration of $i$ in the external phase, kg/m$^3$
$\rho_i^i$ = concentration of $i$ at the interface, kg/m$^3$
$\mu_a$ = dynamic viscosity of air, Pa·s
$AcOH$ = acetic acid
$AcO^-$ = acetate ion
$Chit\text{-}NH_3^+$ = chitosan under soluble form
$Chit\text{-}NH_2$ = chtiosan under gel form
$NH_3$ = ammonia
$NH_4^+$ = ammonium ion
$OH^-$ = hydroxide ion

## Literature Cited


1. Domard A. pH and c.d. measurements on a fully deacetylated chitosan: application to Cu II-polymer interactions. *Int J Biol Macromol*. 1987;9:98–104.
2. Tsukada S, Inoue Y. Conformational properties of chito-oligosaccharides: titration, optical rotation, and carbon-13 N.M.R. studies of chito-oligosaccharides. *Carbohydr Res*. 1981;88:19–38.
3. Mi FL, Shyu SS, Wu YB, Lee ST, Shyong JY, Huang RN. Fabrication and characterization of a sponge-like asymmetric chitosan membrane as a wound dressing. *Biomater*. 2001;22:165–173.
4. Mi FL, Wu YB, Shyu SS, Chao AC, Lai JY, Su CC. Asymmetric chitosan membranes prepared by dry/wet phase separation: a new type of wound dressing for controlled antibacterial release. *J Membr Sci*. 2003;212:237–254.
5. Adekogbe I, Ghanem A. Fabrication and characterization of DTBP-crosslinked chitosan scaffolds for skin tissue engineering. *Biomater*. 2005;26:7241–7250.
6. Kim IY, Yoo MK, Seo JH, Park SS, Na HS, Lee HC, Kim SK and Cho CS. Evaluation of semi-interpenetrating polymer networks composed of chitosan and poloxamer for wound dressing application. *Int J Pharm*. 2007;341:35–43.
7. Boucard N, Viton N, Agay D, Mari E, Roger T, Chancerelle Y, Domard A. The use of physical hydrogels of chitosan for skin regeneration following third-degree burns. *Biomater*. 2007;18:3478–3488.
8. Bansal RC, Donnet JB, Stoeckli F. *Active Carbon*. New York: Marcel Dekker, Inc.; 1988.
9. Boehm HP. Some aspects of the surface chemistry of carbon blacks and other carbons. *Carbon*. 1994;32:759–769.
10. Ania CO, Parra JB, Pis JJ. Influence of oxygen-containing functional groups on active carbon adsorption of selected organic compounds. *Fuel Process Technol*. 2002;79:265–271.
11. Wu FC, Tseng RL, Juang RS. Adsorption of dyes and humic acid from water using chitosan-encapsulated activated carbon. *J Chem Technol Biotechnol*. 2002;77:1269–1279.
12. Babel S, Kurniawan TA. Cr(VI) removal from synthetic wastewater using coconut shell charcoal and commercial activated carbon modified with oxidizing agents and/or chitosan. *Chemosphere*. 2004;54:951–967.
13. Nomanbhay SM, Palanisamy K. Removal of heavy metal from industrial wastewater using chitosan coated oil palm shell charcoal. *Electronic J Biotechol*. 2005;8(1):43–53.
14. Minoura N, Koyano T, Koshizaki N, Umehara H, Nagura M, Kobayashi K. Preparation, properties, and cell attachment/growth behavior of PVA/chitosan-blended hydrogels. *Mater Sci Eng C*. 1998;6:275–280.
15. Ueno H, Yamada H, Tanaka I, Kaba N, Matsuura M, Okumura M, Kadosawa T, Fujinaga T. Accelerating effects of chitosan for healing at early phase of experimental open wound in dogs. *Biomater*. 1999;20:1407–1414.
16. Ishihara M, Nakanishi K, Ono K, Sato M, Kikuchi M, Saito Y, Yura H, Matsui T, Hattori H, Uenoyama M, Kurita A. Photocrosslinkable chitosan as a dressing for wound occlusion and accelerator in healing process. *Biomater*. 2002;23:833–840.
17. Hamilton V, Yuan Y, Rigney DA, Chestnutt BM, Puckett AD, Ong JL, Yang Y, Haggard WO, Elder SH, Bumgardner JD. Bone cell attachment and growth on well-characterized chitosan films. *Polym Int*. 2007;56:641–647.
18. Kiyozumi T, Kanatani Y, Ishihara M, Saitoh D, Shimizu J, Yura H, Suzuki S, Okada Y, Kikuchi M. The effect of chitosan hydrogel containing DMEM/F12 medium on full-thickness skin defects after deep dermal burn. *Burns*. 2007;33:642–648.
19. Ishihara M, Ono K, Sato M, Nakanishi K, Saito Y, Yura H, Kikuchi M, Matsui T, Hattori H, Kikuchi M, Kurita A. Acceleration of wound contraction and healing with a photocrosslinkable chitosan hydrogel. *Wound Rep Reg*. 2001;9:513–521.
20. Thomas S, Fisher B, Fram P, Waring M. Odour absorbing dressings: a comparative laboratory study. *J. Wounds Care*. 1998;7(5):246–250.
21. Köse AA, Karabagli Y, Kürkçüoglu M, Cetin C. Alpha sepiolite: an old clay mineral-a new dressing material. *Wounds*. 2005;17(5):114–121.
22. Ke G, Guan WC, Tang CY, Hu Z, Guan WJ, Zeng DL, Deng F. Covalent modification of multiwalled carbon nanotubes with a low molecular weight chitosan. *Chin Chem Lett*. 2007;18:361–364.
23. Baek SH, Kim B, Suh KD. Chitosan particle/multiwall carbon nanotube composites by electrostatic interactions. *Colloids Surf A Physicochem Eng Aspects*. 2008;316:292–296.
24. Cairns P, Miles MJ, Morris VJ, Ridout MJ, Brownsey GJ, Winter WT. X-ray fibre diffraction studies of chitosan and chitosan gels. *Carbohydr Res*. 1992;235:23–28.
25. Krajewska B. Diffusional properties of chitosan hydrogel membranes. *J Chem Tech Biotechnol*. 2001;76:636–642.
26. Mahdavinia GR, Pourjavadi A, Zohuriaan-Mehr MJ. A convenient one-step preparation of chitosan-poly(sodium acrylate-*co*-acrylamide) hydrogel hybrids with super-swelling properties. *J Appl Polym Sci*. 2006;99:1615–1619.
27. Montembault A, Viton C, Domard A. Physico-chemical studies of the gelation of chitosan in a hydroalcoholic medium. *Biomater*. 2005;26:933–943.
28. Venault A, Vachoud L, Pochat C, Bouyer D, Faur C. Elaboration of chitosan-activated carbon composites for the removal of organic micropollutants from waters. *Environ Technol*. 2008;29(12):1285–1296.

29. Rinaudo M, Pavlov G, Desbrières J. Influence of acetic acid concentration on the solubilization of chitosan. *Polymer*. 1999;40:7029–7032.
30. Chenite A, Gori S, Shive M, Desrosiers E, Buschmann MD. Monolithic gelation of chitosan solutions via enzymatic hydrolysis of urea. *Carbohydr Polym*. 2006;64:419–424.
31. Montembault A, Viton C, Domard A. Rheometric study of the gelation of chitosan in aqueous solution without crosslinking agent. *Biomacromol*. 2005;6:653–662.
32. Han MJ, Bhattacharyya D. Changes in morphology and transport characteristics of polysulfone membranes prepared by different demixing conditions. *J Membr Sci*. 1995;98:191–200.
33. Caquineau H, Menut P, Deratani A, Dupuy C. Influence of the relative humidity on film formation by vapor induced phase separation. *Polym Eng Sci*. 2003;43(4):798–808.
34. Chinpa W, Bouyer D, Pochat-Bohatier C, Deratani A, Dupuy C. Effect of a drying pretreatment on morphology of porous poly(etherimide) membrane prepared using vapor-induced phase separation. *Dry Technol*. 2006;24:1317–1326.
35. Ripoche A, Menut P, Dupuy C, Caquineau H, Deratani A. Poly (ether imide) membrane formation by water vapour induced phase inversion. *Macromol Symp*. 2002;188:37–48.
36. Sun H, Liu S, Ge B, Xing L, Chen G. Cellulose nitrate membrane formation via phase separation induced by penetration of nonsolvent from vapor phase. *J Membr Sci*. 2007;295:2–10.
37. Park HC, Kim YP, Kim HY, Kang YS. Membrane formation by water vapor induced phase inversion, *J Membr Sci*. 1999;156:169–178.
38. Lee HJ, Jung B, Kang YS, Lee H. Phase separation of polymer casting solution by nonsolvent vapor. *J Membr Sci*. 2004;245:103–112.
39. Matsuyama H, Teramoto M, Nakatani R, Maki T. Membrane formation via phase separation induced by penetration of nonsolvent from vapor phase. I. Phase diagram and mass transfer process. *J Appl Polym Sci*. 1999;74:159–170.
40. Khare VP, Greenberg AR, Krantz WB. Vapor-induced phase separation-effect of the humid air exposure step on membrane morphology Part I. Insights from mathematical modeling. *J Membr Sci*. 2005; 258:140–156.
41. Yip Y, McHugh AJ. Modeling and simulation of nonsolvent vapor-induced phase separation. *J Membr Sci*. 2006;271:163–176.
42. Brunauer S, Emmett PH, Teller E. Adsorption of gases in multimolecular layers. *J Am Chem Soc*. 1938;60:309–319.
43. Horvath G, Kawazoe K. Method for the calculation of effective pore size distribution in molecular sieve carbon. *J Chem Eng Jpn*. 1983;16:470–475.
44. Barrett EP, Joyner LG Halenda PP. The determination of pore volumes and area distribution in porous substances. *J Am Chem Soc*. 1951;73:373–380.
45. Kadirvelu K, Faur-Brasquet C, Le Cloirec P. Removal of Cu(II), Pb(II) and Ni(II) by adsorption onto activated carbon cloths. *Langmuir*. 2000;16:8404–8409.
46. Nguyen TTB, Hein S, Ng CH, Stevens WF. Molecular stability of chitosan in acid solutions stored at various conditions. *J Appl Polym Sci*. 2008;107:2588–2593.
47. Vachoud L, Zydowicz N, Domard A. Physicochemical behavior of chitin gels. *Carbohydr. Res*. 2000;326:295–304.
48. Perry RH, Green DW. *Perry's Chemical Engineers' Handbook*. 6th ed. McGraw-Hill; 1984.
49. Gutman M, Nachliel E, Gherson E, Giniger R. Kinetic analysis of the protonation of a surface group of a macromolecule. *Eur J Biochem*. 1983;134:63–69.
50. Zielinski JM, Duda JL. Predicting polymer/solvent diffusion coefficients using free-volume theory. *AIChE J*. 1992;38(3):405–415.
51. Welty JR, Wicks CE, Wilson RE. *Fundamentals of Momentum, Heat, and Mass Transfer*. 3rd ed. New York: John Wiley & Sons, Inc.; 1984.
52. Tsai HA, Kuo CY, Lin JH, Wang DM, Deratani A, Pochat-Bohatier C, Lee KR, Lai JY. Morphology control of polysulfone hollow fiber membranes via water vapor induced phase separation. *J Membr Sci*. 2006;278:390–400.
53. Barreiro-Iglesias R, Coronilla R, Concheiro A, Alvarez-Lorenzo C. Preparation of chitosan beads by simultaneous crosslinking/insolubilization in basic pH Rheological optimization and drug loading/release behavior. *Eur J Pharm Sci*. 2005;24:77–84.
54. Biró E, Németh AS, Sisak C, Feczkó T, Gyenis J. Preparation of chitosan particles suitable for enzyme immobilization. *J Biochem Biophys Methods*. 2008;70:1240–1246.
55. Qin C, Li H, Xiao Q, Liu Y, Zhu J, Du Y. Water-solubility of chitosan and its antimicrobial activity. *Carbohydr Polym*. 2006;63:367–374.
56. Chenite A, Buschmann M, Wang D, Chaput C, Kandani N. Rheological characterization of thermogelling chitosan/glycerol-phosphate solutions. *Carbohydr Polym*. 2001;46:39–47.
57. Park JW, Choi KH, Park KK. Acid-base equilibria and related properties of chitosan. *Bull Korean Chem Soc*. 1983;4(2):68–72.

*Manuscript received May 4, 2009, and revision received July 16, 2009.*